

# MEMS-based Micro-scale Wind Turbines as Energy Harvesters of the Convective Airflows in Microelectronic Circuits

J. Varona\*, R. De Fazio\*\*, R. Velázquez\*, N. I. Giannoccaro\*\*, M. Carrasco\*\*\* and P. Visconti \*\*‡

\*Universidad Panamericana, Facultad de Ingeniería, Aguascalientes, 20290, Mexico

\*\*Department of Innovation Engineering, University of Salento, 73100, Lecce, Italy

\*\*\* Universidad Adolfo Ibáñez, Facultad de Ingeniería y Ciencias, Peñalolén, Santiago 7941169, Chile

(jvarona@up.edu.mx, rvelazquez@up.edu.mx, ivan.giannoccaro@unisalento.it, roberto.defazio@unisalento.it, miguel.carrasco@uai.cl, paolo.visconti@unisalento.it)

‡ Corresponding Author; P. Visconti, Street for Monteroni, Ecotekne University Campus, Tel: +39 0832 297335, ZIP Code 73100, Lecce, Italy, paolo.visconti@unisalento.it

Received: 12.07.2020 Accepted: 14.08.2020

**Abstract-** As an alternative to conventional batteries and other energy scavenging techniques, this paper introduces the idea of using micro-turbines to extract energy from wind forces at the microscale level and to supply power to battery-less microsystems. Fundamental research efforts on the design, fabrication, and test of micro-turbines with blade lengths of just 160 µm are presented in this paper along with analytical models and preliminary experimental results. The proof-of-concept prototypes presented herein were fabricated using a standard polysilicon surface micro-machining silicon technology (PolyMUMPs) and could effectively transform the kinetic energy of the available wind into a torque that might drive an electric generator or directly power supply a micro-mechanical system. Since conventional batteries do not scale-down well to the microscale, wind micro-turbines have the potential for becoming a practical alternative power source for microsystems, as well as for extending the operating range of devices running on batteries.

**Keywords-** Energy harvesting, micro-electro-mechanical system (MEMS), micro-turbine, silicon-based fabrication process.

## 1. Introduction

Advances in integrated circuit (IC) and micro-electro-mechanical systems (MEMS) technologies have enabled the miniaturization and widespread use of mobile devices ubiquitously. However, as systems keep shrinking, the available energy that the traditional batteries can store gets fairly limited, thus further reducing the operating time and portability of such devices. While modern electronics continue to strive for a completely autonomous self-powered microchip and conventional batteries do not scale-down well to the microscale, several approaches for developing micro-power sources have been investigated. Among the different technologies under research are micro-combustors, radioisotope-based generators, electrochemical, and monolithic micro fuel cells [1-7].

Likely, the most viable power supply strategy for realizing autonomous micro-systems (those unattached to an external power supply unit) is the one comprising energy harvesting from the environment and on-board energy storage elements. Energy harvesting refers to the conversion of ambient energy into usable power for a given application [2]. For example, in miniature energy converters, the most typical forms of energy scavenged from the ambient are light, mechanical vibrations, and thermal gradients [4]. The wind is also a very common energy source that has been efficiently harvested for centuries at the macroscale level, but which has received almost no attention for its use in micro-devices [8]. The aim of this research work is to validate the feasibility of developing wind micro-scale turbines as energy harvesters in micro-systems and circuits. Scenarios in which microelectronic chips are exposed to wind forces are common in the automotive and aerospace industries as well

as in applications comprising structure-embedded micro-sensors, mobile devices, etc. There is a variety of micro-circuits and MEMS-based sensor/actuator devices that may benefit from a wind-powered energy source. Moreover, increased transistor count in ICs and multichip modules have led to significant heat density and flux within the microchips. As a result, engineers are faced with never-ending challenges to develop better and more efficient cooling and packaging concepts [9-14]. While traditional cooling systems require extra energy to throw the heat away, there are some initiatives for exploiting the excess heat in ICs as a source of energy to generate electricity. Most of these heat energy scavenging systems are based on the Peltier–Seebeck thermos-electric effect [15-18]. Since current electronic very-large-scale integration (VLSI) Integrated Circuits (ICs) reach power densities over 40 W/cm<sup>2</sup> [19 - 21], there is a potential for extracting energy from convective air currents originated by the heat on the surface of the chips.

Accordingly, this paper presents a study towards developing MEMS turbines that can extract energy from wind forces at the microscale level for powering autonomous and battery-less micro-systems. With a suitable packaging strategy, the wind may come directly from the environment surrounding the microchip or from the convective airflow present in microelectronic circuits and systems. If used in combination with a conventional fan, the experimental micro-turbines cannot only capture a larger amount of wind energy in ICs but enhance the fan's cooling effectiveness by increasing airflow right on the surface of the chip as well.

The manuscript has been organized as follows: Section 2 discusses the main parameters involved in the wind turbine design and presents the conceptual design and modeling of the MEMS turbines herein proposed. Section 3 overviews the fabrication process and characterization of the two developed prototypes. Finally, Section 4 concludes reporting the experimental results and summarizing the main concepts.

## 2. Design Concept and Modeling

The use of heating-induced air currents for powering a turbine is an idea that has been in use for centuries. As hot air has a lower density than the cold one, it naturally rises up creating some wind; this principle is used in passive ventilation systems for buildings where the hot air is exhausted through a turbine that rotates by the wind energy and, once spinning, the blades create a low-pressure region which effectively suctions air to the outside.

More recently, the same principle has been applied to the design of large-scale electric generators, as well as a 200 MW power plant proposed in [22, 23] and similar concepts in [24 - 27]. The system basically comprises a chimney tower and sheets of glass (or plastic) around its base that encloses an expansive surface forming a “heat collection area”, as shown in Figure 1. The air convective movement starts when the air around the tower base is heated by sunlight, causing it to expand and become less dense, and thus more buoyant than cool air in the higher tower portions. [28, 29].

The convective flow moves the heated air upwards as it is simultaneously replaced by the cold air entering at the base

vents by the resulting pressure difference. As air passes up into the tower, it turns turbines that convert the wind force into torque acting on the rotor blades. The turbines in turns power supply an electric generator, which then transfers the obtained power to the grid.

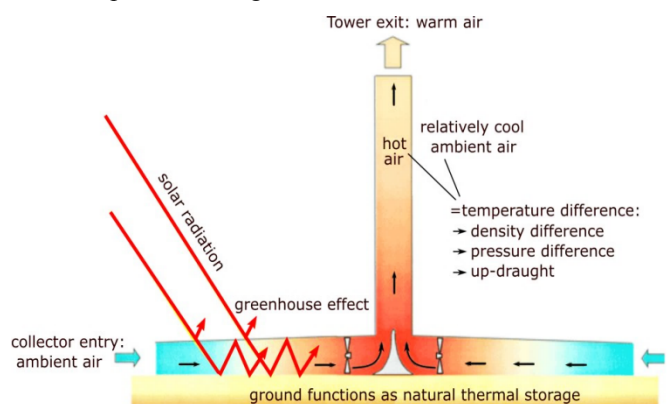


**Fig. 1.** Operation principle of the chimney turbines.

The work herein presented deals with the possibility of using the wind turbines for harvesting, based on the principle described above, energy at the microscale level. The idea is to make productive use of the high heat density available on the ICs surface, transforming it into an energy source. The kinetic energy of wind streams produced by heat on the chip surface is captured by MEMS micro-turbines, so that they are able to drive an electric generator or directly act as a motor for other micro-mechanical devices. Likewise, the MEMS turbines could be used in other applications, where a suitable wind flow is present in the environment [30, 31].

The aerodynamics of wind turbines is quite complex. The airflow and force vary with the length of turbine blades due to the change of angular velocity at each point along the rotating blade. Thus, some calculations used in airfoil design are empirical, while others are based on classical mechanics. Based on Betz's theorem [32], the rotor blades take power from wind by slowing it down and there is both a theoretical and practical limit on the wind energy percentage that can be captured. Numerous methods for the design of wind turbines are available in literature [33-37]. The geometry of optimal wind turbine blade is calculated by sections, considering the variations in airflow as result of rotation. Because the turbine blades themselves are moving, the hitting wind will not come from the direction in which the wind is blowing from the front of the turbine but from an “apparent” direction relative to the speed of each section along the length of the blade as illustrated in Figure 2a. The equations which represent the lift and drag forces are given by Equations (1) and (2):

$$F_{lift} = \frac{1}{2} C_L \rho A V_a^2 \quad (1)$$

$$F_{drag} = \frac{1}{2} C_D \rho A V_a^2 \quad (2)$$

where  $\rho$  is the air density,  $A$  the blade area, and  $V_a$  the apparent wind speed. The lift and drag coefficients,  $C_L$  and  $C_D$ , are dependent on the cross-sectional area of the blades and on the attack angle  $\alpha$  of the apparent wind on the blades.

An airfoil section indicating the chord line and measure of the attack angle  $\alpha$ , is shown in Figure 2b. The chord line is the longest straight line connecting the leading and trailing edges of the airfoil. The lift force on an airfoil increases with  $\alpha$  angle until reaching a point where the airflow over blade surface becomes turbulent and the blade stalls. Beyond the stall point, the lift force falls off quickly and the drag force increases sharply. The rotor blades are designed to have an optimum lift-to-drag ratio until just below stall. Lift and drag coefficients,  $C_L$  and  $C_D$ , for a variety of airfoil shapes are available from experimental data obtained in wind tunnels.

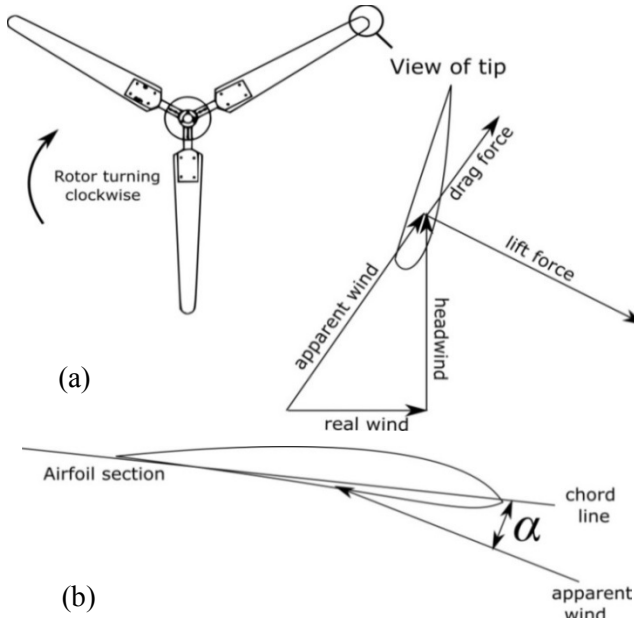


**Fig. 2.** (a) Vector interaction of real incident wind and headwind (due to blade rotation) yields the apparent wind, which defines the actual drag and lift forces at each section along the blade; (b) Angle that the apparent wind direction makes with chord line is referred to as the attack angle ( $\alpha$ ).

In the design of the turbine blades, the exact  $\alpha$  value depends on the angle of apparent wind ( $\phi$ ) and of the blade one ( $\beta$ ). The angle  $\alpha$  is set by the designer to determine the desired lift and drag forces generated in the blade. Figure 3 shows the measurement of the blade angle ( $\beta$ ) in relation to  $\alpha$  and  $\phi$  angles; their relationship is given by Equation (3):

$$\beta = \phi - \alpha \quad (3)$$

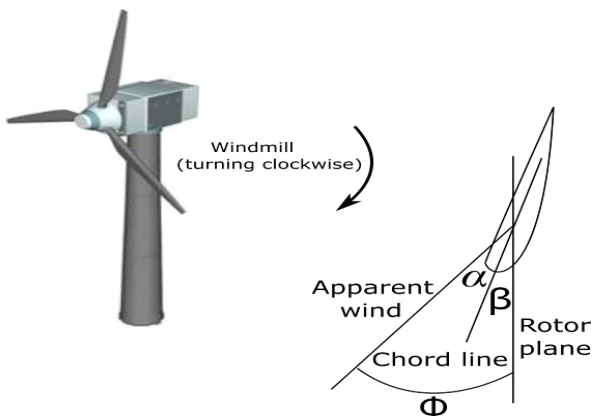


**Fig. 3.** Diagram illustrating the angles  $\phi$ ,  $\alpha$ , and  $\beta$ .

Reference plots and tables are used for calculating the best angle  $\alpha$  for a given lift/drag coefficients ratio. However, most airfoil profiles allow to obtain the maximum efficiency for  $\alpha$  value of  $\sim 5$  degrees; hence Equation (3) becomes:

$$\beta = \phi - 5 \quad (4)$$

For determining the  $\beta$  value, it is necessary to know  $\phi$  value at which the apparent wind reaches the blades. The turbine blades may have different airfoil sections along the blade span, each one optimized for the airflow conditions in each section of the wing. When a blade is rotating, the speed of each section along its length increases from the center of the rotor to the blade tip, as shown in Figure 4. Therefore, the headwind that results from blade rotation is highest at the tip ( $r = R$ ) and the angle of the apparent wind changes at each point along the length; for this reason, the ideal shape of a turbine blade is twisted as depicted in Figure 5.

Based on trigonometric relationship of the wind forces shown in Figure 5, the blade angle  $\beta$  is given by Equation (5) where  $R$  is the blade total length,  $r$  is the position of blade section under consideration along blade span,  $\lambda$  the tip speed ratio, and  $\alpha$  is usually around 5 degrees. The tip speed ratio  $\lambda$  refers to the ratio between the wind speed and speed of the tips of the wind turbine blades, as specified in Equation (6).

$$\beta = \tan^{-1} \left( \frac{2R}{3r\lambda} \right) - \alpha \quad (5)$$

$$\lambda = \frac{\text{Tip\_speed\_of\_blade}}{\text{Wind\_speed}} \quad (6)$$

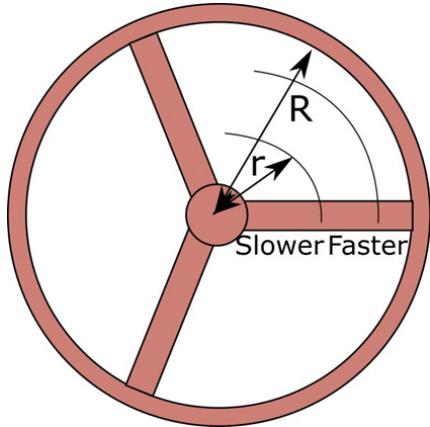


**Fig. 4.** Variation of the angular velocity along the blade span.

The tip speed ratio  $\lambda$  is chosen to maximize the power output and turbine efficiency; usually, a  $\lambda$  value around 5 is used and then optimized empirically. The blade width, or cord width, can also be tapered along the blade span to adjust the amount of wind processed by each blade section in order to satisfy the Betz theorem. Figure 6 shows the area of the rotor plane covered by a blade section with radius  $r$ . The Betz criterion establishes that the wind in each part of the swept area of rotor plane should be slowed down to one-third of its upstream velocity. After mathematical development and simplifications, the chord width for a tapered blade can be approximated by Equation (7), where  $C$  is the chord width as a function of position  $r$  along the blade span,  $R$  is the total blade length from the root to tip,  $\lambda$  is the tip speed ratio, and finally,  $B$  is the number of blades in the turbine rotor.

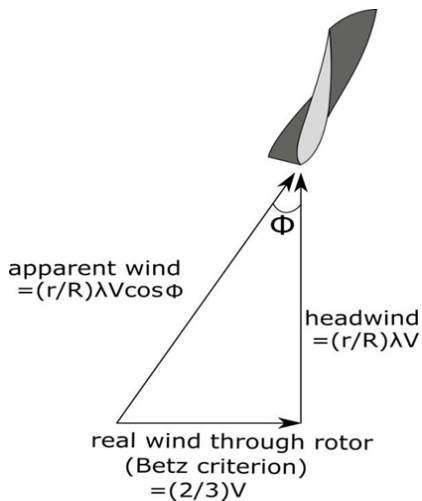


**Fig. 5.** Blade viewed from the tip showing the twist in airfoil orientation.

$$C = \frac{16\pi}{9} \frac{R^2}{r\lambda^2 B} \quad (7)$$

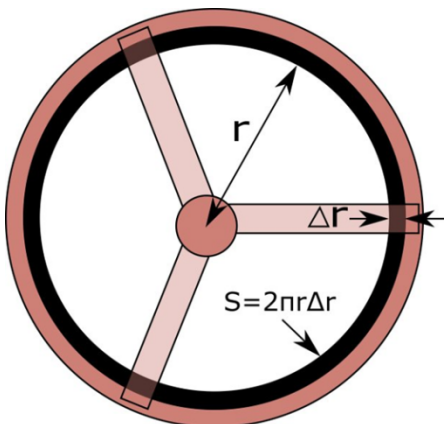


**Fig. 6.** Wind band or rotor area covered by a blade section of width  $\Delta r$  at radius  $r$ .

From Equation (7), it can be observed that the chord width, namely  $C$ , is inversely proportional to radius  $r$ , to the number of blades in the rotor  $B$ , and to the tip ratio squared. In turns, the optimum number of blades is a function of the tip speed ratio as expressed by the following Equation (8):

$$B = \frac{80}{\lambda^2} \quad (8)$$

The flat untwisted blades with constant width and blade angle work well and do not lose much efficiency, but require higher starting torque and suffer more mechanical stress, while a cambered profile blade surely yields a better lift/drag ratio. Depending on the application, the shape of the turbine blades has to be optimized to meet the design specifications.

For the design of MEMS micro-scale wind turbines, several additional constraints must be considered. First, the use of a MEMS fabrication process imposes severe manufacturability restrictions as the number of structural layers, their nominal thickness, as well as material properties have to be all defined by the process and cannot be changed. Secondly, there is little information available on the typical characteristics of airflow over a microchip substrate and

some important design parameters such as the wind speed are unknown. Furthermore, the structures created through the MEMS micromachining processes are inherently limited to two-dimensions (2D) or to 2.5D at most (considering the fixed thicknesses of the deposited material films), whereas the complex tri-dimensional (3D) shapes of macro-scale blades cannot be accomplished in classical MEMS.

Yet, due to the great commercial demands for simplified device structures compatible with low-cost and mass-production microelectronic manufacturing technologies, the standard Poly-silicon Multi-User MEMS process (Poly-MUMPS) [38] without special post-processing steps was chosen for the economic development of the micro-turbine prototypes proposed in this research work. Poly-MUMPS process methodology offers three layers of polysilicon (Poly) and two sacrificial layers of phosphor-silicate glass on an insulating film of silicon nitride. The last two poly-silicon layers are releasable. A gold layer can be evaporated onto the surface at the end of the process by low-pressure chemical vapor deposition (CVD) [39]. The thickness of each material film is summarized in the following Table I [40]. After the construction, the sacrificial layers are removed in a bath of buffered hydrofluoric acid (HF) acid [41].

**Table 1.** Poly-MUMPS Process: Materials and Thickness.

Material Layer	Thickness (μm)
Nitride (silicon nitride)	0.6
Poly-0 (non-releasable)	0.5
Oxide-1 (phospho-silicate glass)	2.0
Poly-1 (releasable)	2.0
Oxide-2 (phospho-silicate glass)	0.75
Poly-2 (releasable)	1.5
Metal (gold)	0.5

Two initial concepts were proposed for developing a MEMS wind micro-turbine. The first one is inspired by the operation of ventilation turbines; in this case, the second and third layers of poly-silicon (*Poly1* and *Poly2* layers, respectively) were used for building the rotor and blade structures. The central hub on the *Poly2* layer was anchored to the substrate of the chip. As the micro-turbine begins its rotation and the hot air escapes from the surface area enclosed beneath the rotor, the generation of breezes may be further favored. A potential increase in air circulation on the surface of the chip could also help by removing excess heat in micro-cooling systems. The design of this micro-scale wind turbine is depicted in the following Figure 7(a).

As shown in Figure 7(a), the *Poly2* layer is used for realizing the blades of the turbine, by extending them from its *Poly1* skeleton. The chord width was tapered from the root to the tip of the blade going from 22 to 70 μm. Except for the leading edge, where *Poly1* layer is present, the blades are essentially flat on *Poly2* with an angle  $\beta$  of 0°. A length of  $R$  equal to 160 μm was chosen along with eight blades ( $B = 8$ ), anticipating low tip speed ratios and moderate winds.

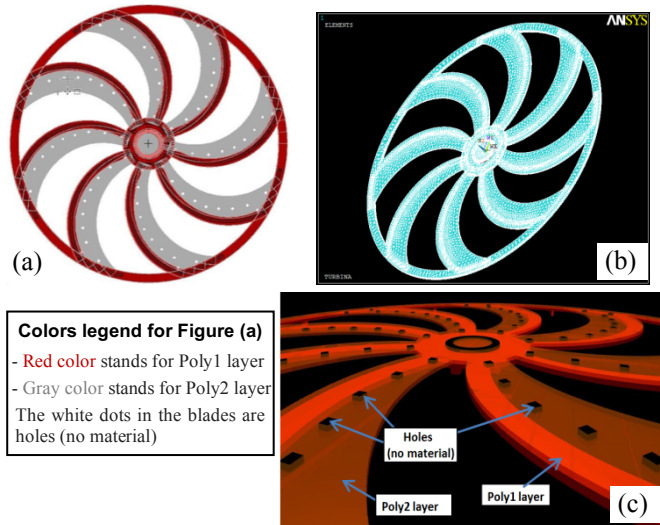


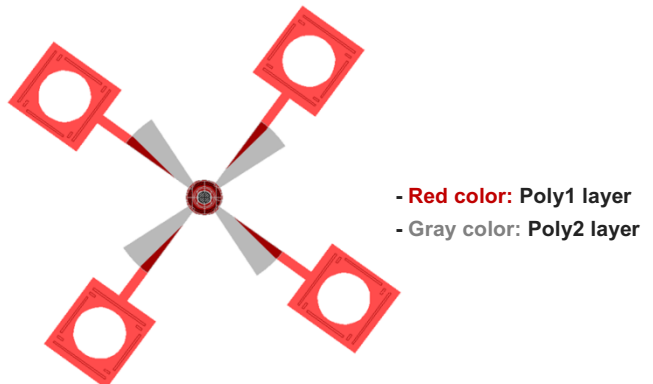
**Fig. 7.** (a) Top view of the conceptual “ventilation” micro-turbine; (b) Its finite element model (FEM) by means of the Ansys software; (c) Three-dimensional model of the micro-turbine with visible blade details.

A second approach considers the use of a four-blade micro-turbine resembling the design of old windmills used to lift weights, grind grain, or pump water. The angle of the blades equals zero (namely,  $\beta=0$ ), mainly due to the fabrication process constraints. The blades were linearly tapered and the chord width was made relatively large in order to capture a larger amount of air, assuming that the rotating speed is quite low. Each blade spans  $160 \mu\text{m}$  from the root to tip and it was built on *Poly2* layer alone. The model of this turbine is presented in the following Figure 8.

An important difference between the two turbines is that in the “windmill” design the blades are not flat but semi-twisted. An original technique presented in [38] that extends the capabilities of standard surface micromachining MEMS processes to form three-dimensional structures was used for providing the blades with a non-flat profile and thus improving the lift/drag ratio of the system. Further details of this fabrication are presented in Section 3. Both micro-turbine prototypes were analyzed and verified by using three-dimensional finite element models (FEM) carried out with Ansys software. The ventilation-type turbine FEM is shown in Figure 7(b). FEM simulations through the Ansys software allowed us to optimize the geometry and mechanical structure of both the proposed models of micro-turbines (as shown for example in the micro-turbine 3D model of Figure 7(c) with a magnification of the blade details), and then proceed with the fabrication process as described below.

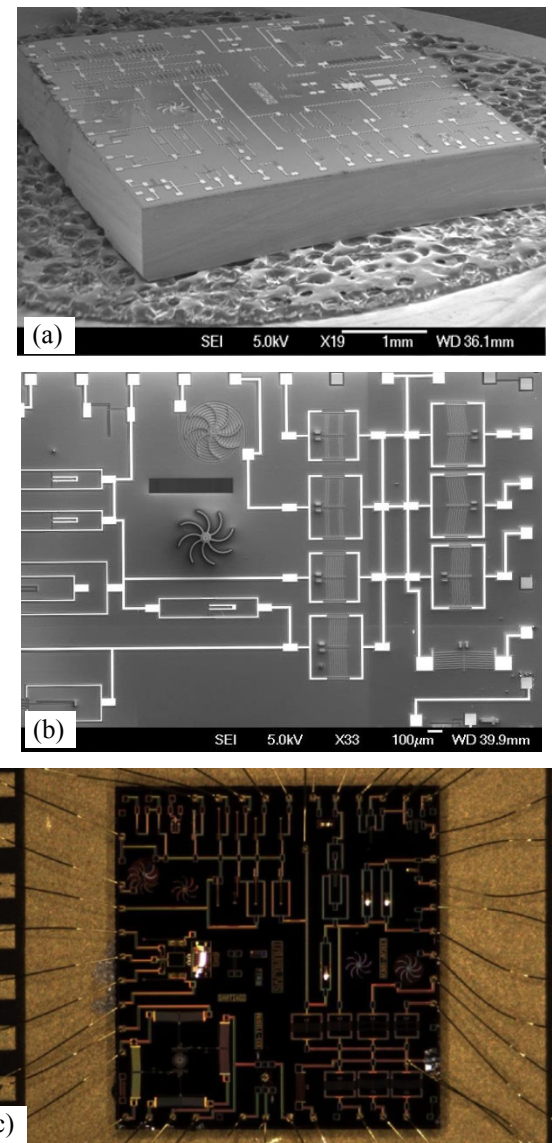
### 3. Details on micro-turbines fabrication, experimental setup and characterization

The micro-turbines were fabricated using the standard and commercially available multi-user MEMS poly-silicon process (PolyMUMPs) [38]. In order to reduce the friction, dimples were used on the blades to minimize the amount of poly-silicon in direct contact with the silicon nitride layer over the chip substrate. After fabrication, the devices were released by removing the sacrificial Phospho-silicate glass (PSG) layer in a solution of buffered hydrofluoric acid (HF).



**Fig. 8.** Top view of the windmill-type micro-turbine.

In the following Figures 9 and 10, several Scanning Electron microscope (SEM) images of the fabricated micro-turbines prototypes (of both ventilation and windmill types) are shown with different magnifications. In particular, in Figures 9(a-c), a silicon chip with different MEMS structures on board is shown, electrically wire bonded to the external pads in order to extract the obtained electrical signals from MEMS-based micro-generators or to drive the MEMS structures (e.g the serpentine micro-scale actuators).



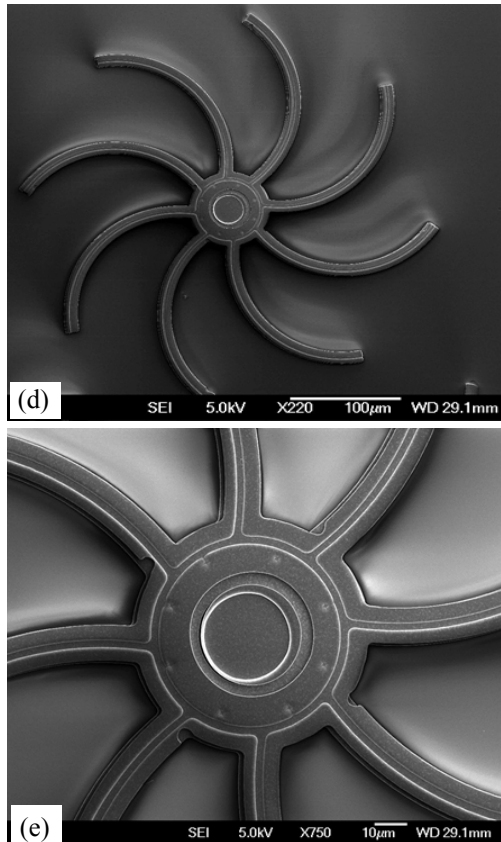


**Fig. 9.** SEM images of silicon chip with MEMS ventilation-type micro-turbines on board (a-b); packaged chip bonded by gold wires to the external pads (c), and magnified images of the micro-scale polysilicon-made realized turbines (d and e).

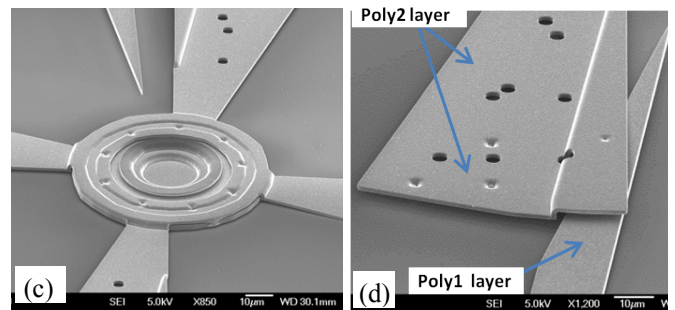
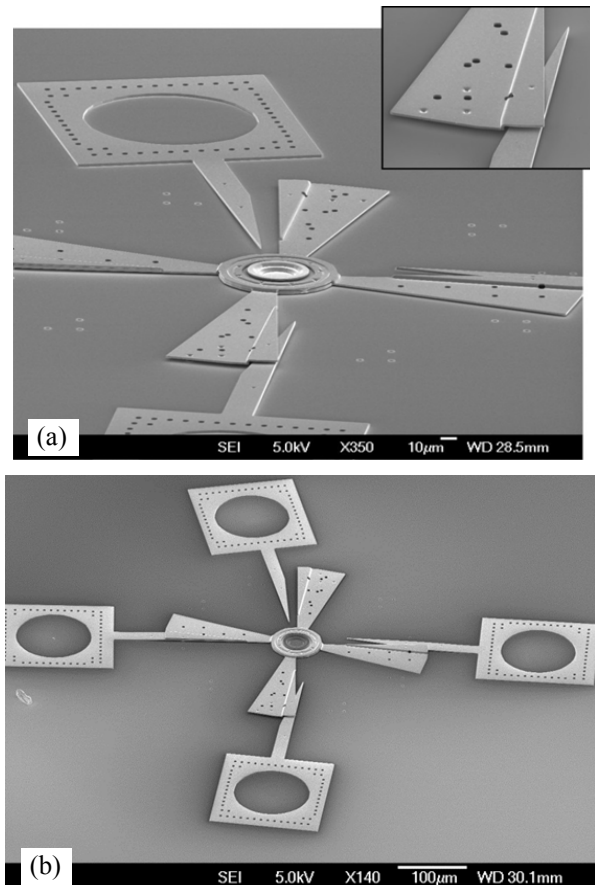
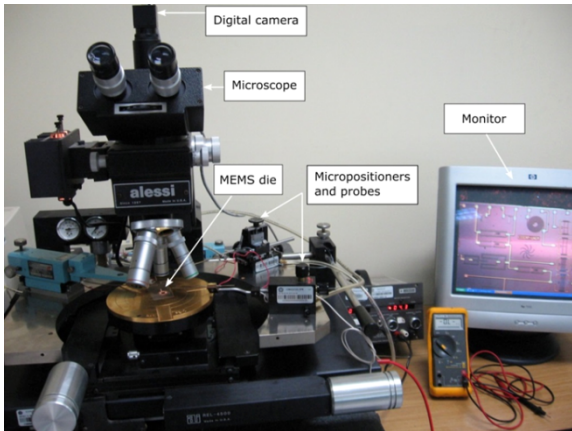


**Fig. 10.** Scanning electron microscope (SEM) images of the windmill-type microturbine with different magnifications (a-c); close-up view of the blade profile with the tip of dummy Poly1 object (to be removed) visible under the blade (d).

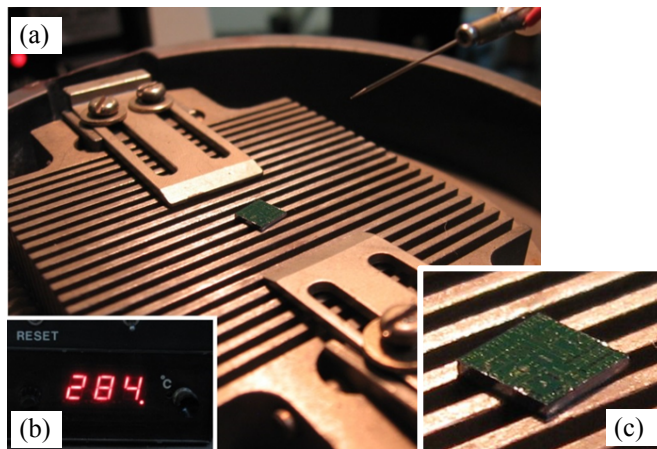
As mentioned earlier, the blade profile of the windmill micro-turbine is not flat but slightly shaped to obtain an improved lift/drag ratio ( $C_L/C_D$ ) of the cambered airfoil. Figure 10(d) shows the detail of the blade profile where 3D twist of the poly2 layer can be appreciated. The technique for producing 3D shapes from a single flat thin polysilicon film [38] leverages the coplanar nature of the MUMPs fabrication process where the topography of the upper layers depends on the patterns of structural and sacrificial layers underneath. Therefore, dummy structures are placed underneath the layer of interest to create a desired shape in the vertical plane. Accordingly, a dummy structure in the *Poly1* layer was built under *Poly2* blades of the turbine for producing the desired pattern on the blade profile. Once the sacrificial oxide layers are removed after fabrication, these dummy structures will not play any role in the operation of realized micro-turbine and can be easily removed if necessary [43, 44].

Figure 11 presents the general test setup used for testing the turbines. Temperatures in excess of 100 °C are fairly common in environments where MEMS-based devices find practical use; examples include the automotive and aerospace industry where high heat transfer rates and temperatures beyond 500 °C are commonly available [45, 46]. Therefore, the entire microchip was gradually brought up to a temperature of 300 °C, with incremental steps of 20 °C, using an electric heating resistor connected to a thermometer, as shown in the experimental measuring setup shown in Figure 12a. The chip was then placed under the microscope to inspect the response of the turbines to the thermally induced wind flow created on the surface of the chip. For this purpose, an RGB high-resolution digital camera was coupled to the microscope in order to record the 30 seconds long videos of rotating micro-turbines, at all temperatures shown in Figure 13 with increments of 20 degrees each time, for the subsequent off-line processing. The limit of 300 °C used in these tests was set based on average temperatures that can be found in electronic VLSI integrated circuits (ICs), which may have power densities above 40 W/cm<sup>2</sup> [20, 21], as well as in thermally actuated MEMS-based devices [46, 47].

Figure 13 shows the experimental relation between the microchip temperature and rotational speed in the windmill-type tested micro-turbine. The rotational speed was measured by processing the video frames recorded by the camera at each temperature value. At first, the turbines did not move which suggests that they require higher starting torque.



**Fig. 11.** General test bench used for experimentation and characterization of the realized MEMS turbines.



**Figure 12.** Testing experimental setup by a resistive heater to increase the microchip temperature (a); indication of the temperature reached by heater and measured by thermometer (b); chip magnification with micro-turbines on board to harvest energy from convective airflow due to heating.

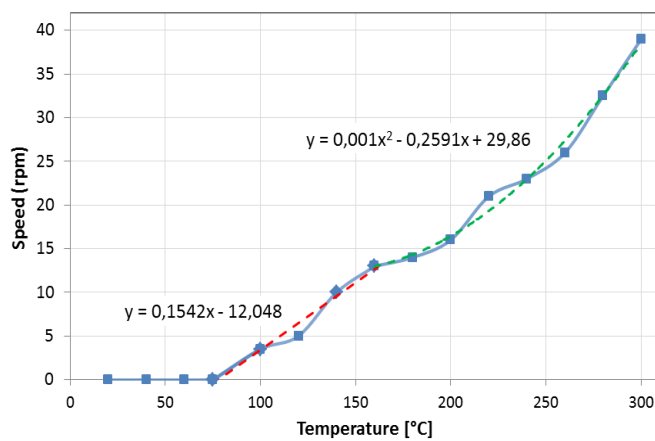


**Fig. 13.** Experimental relation between the windmill-type micro-turbine rotational speed and microchip temperature.

However, if a micro-probe is used to initiate the rotation of the turbine blades and a fan is positioned over the chip (like in a forced convection situation), then the movement is sustained beyond the momentum produced by the micro-probe impulse, by achieving rotational speeds of about 40 rpm when heated up to 300 °C. This is an indication that the

micro-turbine is extracting energy from created convective airflow and the concept herein presented is empirically validated. As shown in Figure 13, the tested micro-turbine does not exhibit any rotational motion up to 75 °C (even with the microprobe impulse); then, starting from 75 °C, the rotation speed of the micro-turbine blades becomes higher as the temperature increases; as evident from the graph, two distinct trends are present, namely a linear one from 75 to 160 °C and a quadratic one in the range 160 °C - 300°C.

The mass measurement in MEMS structures is naturally complex due to the scale and the unavailability of specialized equipment. For estimating the total mass ( $m_t$ ) of the device, it is necessary to calculate the mass of each blade and that of the rotor as described by Equation (9), where  $m_t$  represents the total mass of the device,  $m_c$  the mass of central rotor,  $m_b$  the mass of each blade, and  $m_e$  the mass that takes into account the irregularity of the profile at the extremity of each blade. Each mass can be represented in terms of its volume and material density ( $\rho$ ). Thus, Equation (9) can be expressed as Equation (10), where  $\rho_{poly}$  is the density of polysilicon material (2330 kg/m<sup>3</sup>), while  $V_c$ ,  $V_b$ , and  $V_e$  are the volumes of the central rotor, of the blade, and of the equivalent additional surface at the blade extremity, respectively.

$$m_t = m_c + 4m_b + 4m_e \quad (9)$$

$$m_t = \rho_{poly}(V_c + 4V_b + 4V_e) \quad (10)$$

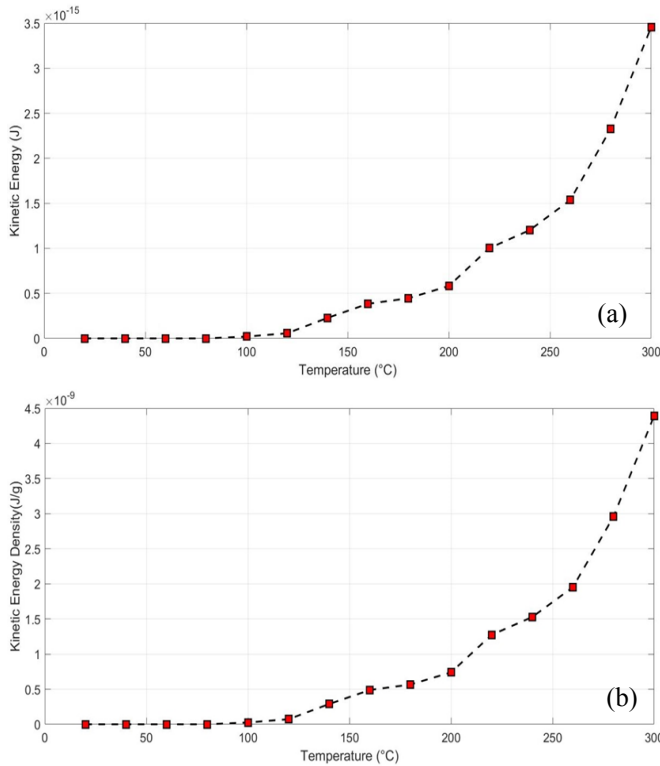
The dimensions are naturally known and assuming a constant material density along the temperature range considered, the total mass of the windmill-type micro-turbine prototype can be estimated in about 15 µg (taking into account an uncertainty of 1-2% on the dimensions deriving from the turbine fabrication process). From the knowledge of the geometry, the device inertia ( $I$ ) has been estimated equal to  $4.15 \cdot 10^{-16}$  kg m<sup>2</sup> by using the simplified Equation (11); here,  $r_b$  and  $r_c$  are the length of the blades (160 µm) and the radius of the central rotor (35 µm), respectively.

$$I = \frac{4}{3}m_b r_b^2 + \frac{1}{2}m_c r_c^2 + 4m_e r_c^2 \quad (11)$$

Then, the kinetic energy  $E_c$  of the rotating windmill has been calculated by the following Equation (12), where  $\omega$  is the angular (rotational) speed expressed in rad/sec.

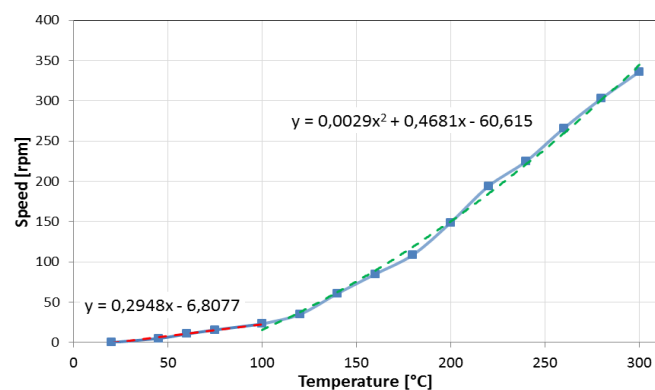
$$E_c = \frac{1}{2} \cdot I \cdot \omega^2 \quad (12)$$

Figure 14(a) shows the kinetic energy  $E_c$  of the rotating windmill-type micro-turbine as a function of temperature (on the basis of the angular velocity values shown in Figure 13, expressed in rpm); the turbine is capable of acquiring a maximum kinetic energy of  $3.5 \times 10^{-15}$  J, in environments exhibiting 300 °C, which can then be transferred to other devices (possibly transforming it into electric charge) to be exploited. Figure 14(b) shows the ratio of the kinetic energy ( $E_c$ ) with the total mass of the micro-turbine as a function of the temperature, in order to obtain a normalization of the kinetic energy with the mass of the device. The normalized parameter could be useful for comparing the performances of proposed micro-device with other existing systems.



**Fig. 14.** Kinetic energy of the windmill-type micro-turbine as a function of temperature.

Furthermore, in Figure 15 the experimental results related to the characterization of the ventilation-type micro-turbine are reported, showing the rotation speed trend as a function of the chip temperature. As evident, for a given temperature, the rotational speed is much higher (more than an order of magnitude) compared to the windmill-type micro-turbine; this can be explained with a higher number of blades of the ventilation-type turbine respect to the windmill-type one, with the greater area and lift and drag coefficients featuring the blades' profile of the ventilation-type design.



**Fig. 15.** Experimental relation between the ventilation-type turbines rotational speed and the microchip temperature.

Based on results above reported, the kinetic energy ( $E_c$ ) of the ventilation-type turbine as a function of temperature has been calculated (Figure 16) by using Equation (12) and estimating the inertia ( $I$ ) of the ventilation-type structure, equal to  $3.62 \times 10^{-15}$  kg m<sup>2</sup> from geometrical considerations similar to those previously done for ventilation-type design.

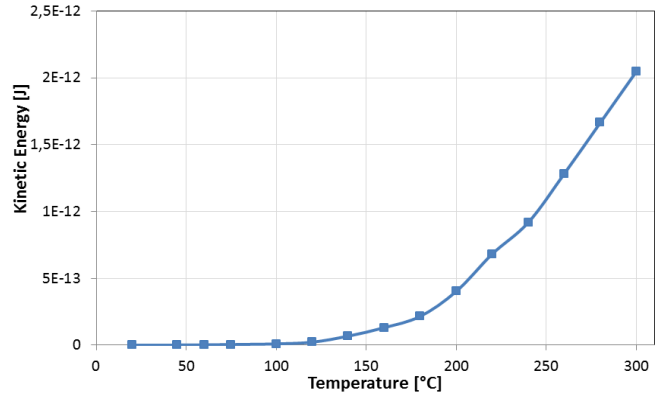


**Fig. 16.** Kinetic energy of the ventilation-type micro-turbine as a function of temperature.

As can be noted, for a temperature of 300 °C, the ventilation-type micro-turbine provides a kinetic energy equal to  $2.05 \times 10^{-12}$  J, much higher than those obtained for the windmill-type one for the same chip temperature, a result due to the greater rotational speed and moment of inertia featuring the ventilation-type micro-turbine.

Note that the  $E_c$  magnitude is indeed low when compared to active (i.e. powered) millimetric turbines that can exhibit magnitudes in the order of hundreds of  $\mu$ J; scaling dimensions down to micrometers and passively powering the device, its kinetic energy dramatically reduces. However, the micrometer concept here proposed is not intended to be used as a stand-alone device; it is expected to build monolithic blocks containing several micro-turbines that can work altogether, thus increasing the overall performance in terms of the harvested energy. Figure 17 shows the conceptual representation of a 3 x 3 block; it can fit in a square of 1 mm<sup>2</sup> as well as centimeter-scale custom-designed similar blocks can be designed to be placed over the ICs, to exploit their over-heating.

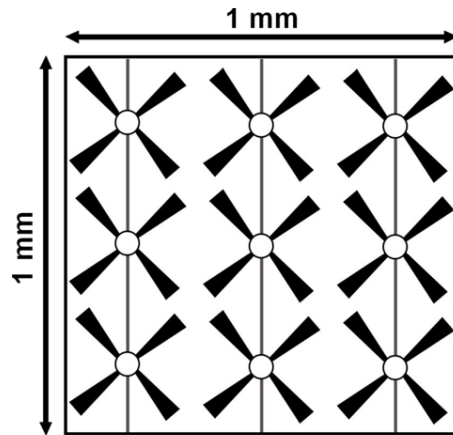


**Fig. 17.** Depiction of a monolithic block integrating 9 windmill-type micro-turbines.

#### 4. Results discussion and future developments

This experimental setup, however, does not model accurately the conditions encountered inside a packaged chip. The loose and naked die over the heating device (as shown in Figure 12a) is immersed into what appears to be an “infinite” mass of cold air in the lab area and airflow

produced by the fan escapes in multiple directions. Therefore, further refinement of the testing conditions and the experimental setup is required, including testing of the realized micro-turbines inside a packaged chip that is not exposed directly to cooler air mass from the surroundings and that confines the thermally induced winds within the surface of the chip itself. In addition, the micro-turbines have yet to be tested under airflow conditions, which may come from various sources, different respect to convective airflow caused by the heating of the chip surface, like for example forced convective winds applied on the chip, etc.

In this initial activity of characterization and testing of micro-turbines, the main objective was to validate experimentally the thermodynamic and aerodynamic cycles at the micro-scale level, so identifying the limitations and potential advantages that may be used for developing and optimizing the micro-scale turbines, to be used as wind harvester embedded in microelectronic circuits and systems. Such devices may find applications as a power source for autonomous sensors, circuits, and other micro-systems in a variety of practical situations where air flux is commonly available (e.g. sensors and circuits used in the automotive and aerospace industries, etc.). Some previously proposed micro-mechanisms that could apply the results being developed in this work include high mobility small rovers, miniaturized Stirling engines, MEMS power generators, implantable biosensors, and other heat engines [48 - 57].

The application of micro-turbines to energy harvesting has attracted the attention of the scientific community from the past few decades [58-63], for implementing compact and efficient solutions for scavenging energy from fluid flow, such as wind, sea currents, breathing, etc [48-52]. F. Herrault et al. developed and tested millimeter-scale electromagnetic generators, featured by different geometric configurations as well as the number of poles and turns of the magnetic rotor [53]. They demonstrated that, for a four-pole and six-turns NdFeB generator, 6.6 mW<sub>rms</sub> maximum power was obtained with a 1.8 Ω load resistor at 392.000 rpm. In this context, M. Kaneko et al. presented three types of MEMS air turbine generators, different for the bearing system, configuration of the magnetic circuit, and shape of the rotor [54]. In particular, the generator with the rim-type rotor and miniaturized ball bearing reached higher rotational speed (up to 290.135 rpm) compared to the configurations with flat-rotor, both with fluid dynamic bearing or miniature ball bearing systems. The first turbine type was combined with a magnetic circuit realized by multilayer ceramic technology; the resulting inductive generator provides 2.41 mVA output power with 8 Ω load resistance and 139 mV, respectively.

In the reference [55], the authors developed a miniaturized electromagnetic generator constituted by a MEMS air turbine and a three-phase magnetic circuit, made with ceramic technology; this last, based on Ni-Cu-Zn magnetic material and silver paste for the coils, showed very low DC resistance. The resulting three-phase generator achieved a maximum output power of 3.01 mVA, with a flow rate of 2.9 l/min and 3 Ω load resistance. In the reference [57], the authors proposed two types of miniaturized electromagnetic power generators, all

constituted by a MEMS-based air turbine and a magnetic circuit realized with multilayer ceramic technology and silver paste; specifically, the first generator is single-phase type MEMS air turbine generator, whereas the latter three-phase type. The performance of the magnetic circuit alone has been determined by using a rotating permanent magnet attached to a spindle machine; in this case, the single-phase generator showed a maximum output power of 1.47 mVA with a rotational speed of 380.000 rpm and a load resistance of 1 Ω, while the three-phase one provided 3.3 mVA under the same conditions. Instead, by placing the MEMS air turbine, the output power was only 1.74 μVA (with rotational speed of 30.000 rpm) and 1.41 μVA (with rotational speed of 18.000 rpm), respectively for the two types of generators.

Given the developed micro-turbine in this research work, the most suitable harvesting strategy for scavenging energy from the convective flow due to temperature gradient on the chip is the electromagnetic induction technology. In particular, the miniaturized generator to be applied to the rotating micro-turbine is depicted in Figure 18(a); it includes a two-pole coil structure placed on a magnetic layer, connected in a vertical way through a connected layer. The magnetic material is a ceramic one (co-fired NiCuZn ferrite) featured by a relative magnetic permeability value equal to 900, whereas low-resistance silver conductive paste is used for the coil (Figure 18(b)). Once the magnetic circuit and air turbine are put together, the magnet connected to the air turbine shaft is located between the magnetic material layers; in this way, a time-varying magnetic field is induced in the two coils, thus producing an alternate voltage on their terminals. Therefore, a proper conditioning section is needed to adapt the voltage provided by the energy generator to that required by the employed storage device.

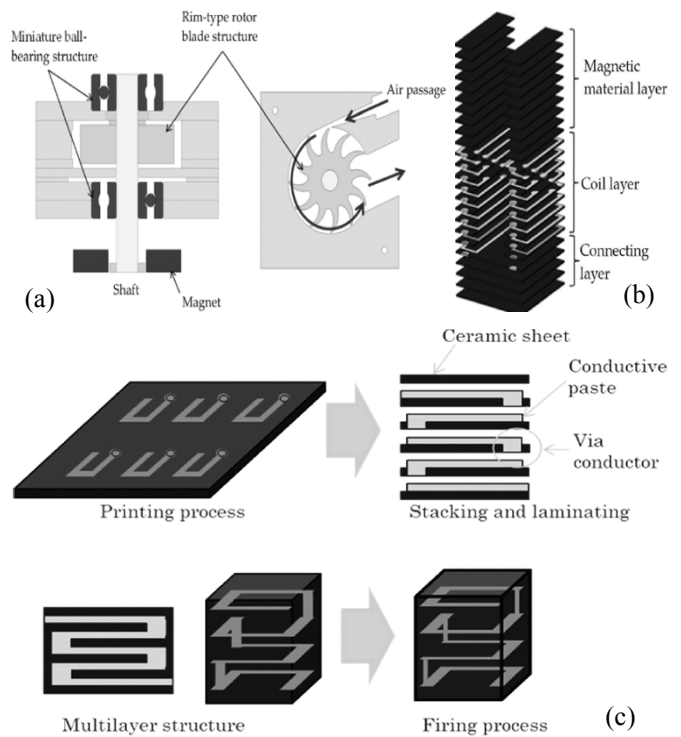


**Fig. 18.** Structure of the developed magnetic-inductive harvester (a); detail of the two-pole coil structure (b), the fabrication process of the multilayer magnetic circuit [54].

The fabrication process of the magnetic circuit is shown in Figure 18(c); the substrate is constituted by a ceramic multi-layer structure, as well as the coil pattern is deposited, using silver paste, by employing the screen printing technology. The through-holes for connecting the underlying layer were realized by the etching process [64] and after filled by the conductive paste [60]. The coil sheets were stacked and connected to each other by a laminating process.

Afterward, the maximum electrical power that can be extracted from the harvesting system, for both micro-turbine typologies, was estimated. Considering a 60% conversion efficiency for the electro-magnetic generator as reported in literature for similar micro-generators [65], and experimental results shown in Figures 14 and 16, the maximum power for a single micro-generator including a windmill-type turbine is equal to  $2.1 \times 10^{-15}$  VA (for a rotation speed of 30 rpm), as well as for the ventilation-type one, the generator provides at most  $1.23 \times 10^{-12}$  VA (for a rotation speed of 336 rpm). Despite the low power obtained values, the low size allows the integration of a multitude of these devices in unused areas of the silicon chip leading to scavenge a considerable amount of energy that would otherwise be wasted, usable for reducing the energy requirement of the chip.

Comparing these results with those previously reported in [57], it is necessary to point out that the turbines characterized in [57] had a mm-scale size (about an order of magnitude larger than those realized and tested in this work). Besides, the rotation speed is 2 orders of magnitude greater than that obtained in our experiments, since the airflow is not determined by a conventional fan but induced by the heating of micro-chip determined, in the integrated circuits, by the dissipation of the electrical power. An important advantage of the proposed MEMS-based harvesting system is that each micro-turbine is very light with an optimized geometry, so allowing energy production also with the very weak wind-flow, determined by heating the silicon chip, investing each realized micro-turbine.

To better underline the potential of proposed micro-turbines, it is possible to consider a block of 1 cm x 1 cm that, with the arrangement shown in Fig. 17, can contain 900 turbines. Hence, by considering the obtained results related to the ventilation-type micro-turbines (i.e. harvested electrical power of 1.23 pVA) with only the excitation of the thermally-induced airflow ( $T = 300$  °C and turbine rotation speed = 336 rpm), an overall power of 1.1  $\mu$ W can be extracted. This result is extremely satisfactory and opens up new usage scenarios; in fact, it is possible to predict that, with more intense air flows due, for instance, to the race of person wearing wearable devices [66], environmental or industrial vibrations as well as goods transportation [67], the turbines rotation speed will reach much higher values as well as the produced electrical power.

In conclusion, the idea of using MEMS micro-turbines to capture energy from the heating-induced wind at the micro-scale was presented in this work. While prototypes have been demonstrated, further design enhancements and optimizations are required for the micro-turbines to become of practical use. In consideration of manufacturability and cost, the proposed devices have been fabricated by using a

standard surface micro-machining silicon-based process. The blades geometry while subject to capabilities and limitations of the MEMS process, was designed to present a non-flat airfoil profile akin to large-scale high-performance rotors.

## 5. Conclusion

Although this research is still in the early testing stages for proof-of-concept, the preliminary results presented in this work show the great potential that the micro-turbines have for becoming one of the most significant advancements in power generation and energy harvesting at the microscale level. Several opportunities for design improvements have been identified and a second set of turbine prototypes is under development. Future improvements will focus on achieving a lower starting torque and optimizing airfoil shape to yield a higher lift/drag ratio. Energy harvesters find a broad range of applications in the development of complex and autonomous micro-systems and circuits. Furthermore, innovations in the area of micro-power generation, that may increase the operation time of portable devices and reduce the number of required batteries, has a huge market potential.

## References

- [1] S. A. Jacobson and A. H. Epstein, "An informal survey of power MEMS", in Proceeding of Int. Symp. on Micro-Mechanical Engineering ISMME 2003, pp. 1-8, 2003.
- [2] T. Ishiyama, "Output Characteristics of Energy Harvesting Using Multiple Energy Sources", in IEEE Proceeding of 2019 8th Int. Conference on Renewable Energy Research and Applications (ICRERA), 3-6 Nov. 2019, Brasov – Romania, pp. 224 - 228, 2019, DOI: 10.1109/ICRERA47325.2019.8996552.
- [3] G. Hang and A. Lal, "Self-reciprocating radioisotope-powered cantilever", Journal of Applied Physics, vol. 92, no. 2, pp 1122-1127, July 2002.
- [4] D. Ryan and R. LaFollette, "Power supply and energy storage for autonomous MEMS", Journal of Aerospace, vol. 109 (1), pp. 870-874, 2000.
- [5] G. Maruccio, P. Visconti, S. D'Amico, R. Cingolani, R. Rinaldi, "Planar nanotips as probes for transport experiments in molecules", Microelectronic Engineering, vol. 67-68 C, pp. 838-844, 2003.
- [6] K.B. Lam, E.A. Johnson, C. Mu, L. Liwei, "A MEMS photosynthetic electrochemical cell powered by subcellular plant photosystems", J. of Microelectr. Systems, vol. 15 (5), pp. 1243-1250, (2006).
- [7] N. Torres-Herrero, J. Santander, N. Sabate, J.P. Esquivel, A. Tarancón, I. Garbayo, I. Gracia, C. Cane, "Monolithic micro fuel cells as integrated power sources in MEMS", in Proc. of IEEE Spanish Conf. on Electron Devices, Santiago de Compostela, pp. 412-415, 2009.
- [8] G. Acciani, F. Di Modugno, G. Gelao and E. Mininno, "Shape optimization of cantilever beam for wind energy harvesting", in IEEE Proceeding of 2015 Int. Conference on Renewable Energy Research and Applications

- (ICRERA), Palermo, 2015, pp. 1207-1212, DOI: 10.1109/ICRERA.2015.7418600.
- [9] D. B. Go, S. V. Garimella, T. S. Fisher and R. K. Mongia, "Ionic winds for locally enhanced cooling", Journal of Applied Physics, vol. 102, pp. 1-8, 2007.
- [10] C.H. Amon, S.C. Yao, C.F. Wu, C.C. Hsieh, "Micro-electromechanical system-based evaporative thermal management of high heat flux electronics", ASME Journal of Heat Transfer, vol. 127, pp. 66-75, 2005.
- [11] Y. Cheng, Y. Xu, D. Zhu, W. Zhu, L. Luo, "Thermal analysis for indirect liquid cooled multichip module using computational fluid dynamic simulation and response surface methodology", IEEE Trans. on Components and Packaging Technologies, vol. 29 (1), pp. 39-46, 2006.
- [12] P. Primiceri, R. de Fazio, P. Carlucci, P. Visconti, "Photo induced ignition phenomenon of Carbon nanotubes by Xenon pulsed light: ignition tests analysis, automotive and new potential applications, future developments", J. Applied Research Tech. vol. 15(6), pp. 609–623, 2017.
- [13] J. Li, G.P. Peterson., "Geometric optimization of a micro heat sink with liquid flow", IEEE Trans. on Components and Packaging Techn., vol. 29 (1), pp. 145-154, 2006.
- [14] M. S. Bakir, G. Huang, D. Sekar, and C. King, "3D integrated circuits: liquid cooling and power delivery", IETE Technical Review, vol. 26 (6), pp. 407-416, 2014.
- [15] R. Sing, J. Nurnus, Z. Bian, J. Christofferson, A. Shakouri, "Temperature profile inside microscale thermoelectric module acquired using near-infared thermoreflectance", IEEE Trans. on Components and Packaging Technologies, vol. 32 (2), pp. 447-452, 2009.
- [16] H. Lhermet, C. Condemeine, M. Plissonnier, R. Salot, P. Audebert and M. Rosset, "Efficient power management circuit: from thermal energy harvesting to above-IC microbattery energy storage", IEEE Journal of Solid-State Circuits, vol. 43 (1), pp. 246-255, 2008.
- [17] R. de Fazio, D. Cafagna, G. Marcuccio, P. Visconti, "Limitations and Characterization of Energy Storage Devices for Harvesting Applications", Energies, vol. 13 (4), pp. 1 - 19, 2020.
- [18] P. Visconti, P. Primiceri, R. Ferri, M. Pucciarelli, E. Venere; "An overview on state-of-art energy harvesting techniques and related choice criteria: a WSN node for goods transport and storage powered by a smart solar-based EH system", Int. Journal of Renewable Energy Research, vol. 7 (3), pp. 1281-1295, 2017.
- [19] J. Varona, R. Velazquez, M. Tecpoyotl, "Design of baseband digital delta-sigma modulators in 180nm CMOS", IEEE Latin America Transactions, vol. 13 (5), pp. 1272-1278, 2015.
- [20] M. Pedram, S. Nazarian, "Thermal modeling analysis and management in VLSI circuits: principles and methods", Proceeding of IEEE, vol. 94 (8), pp 1487-1501, 2006.
- [21] Li Jiang, J. M. Zhou, C. G. Li, "Estimate of the power dissipation of multilayer and high density nano-CMOS chip", in Proceeding of IEEE 2005 Conference on High Density Microsystem Design and Packaging and Component Failure Analysis, Shanghai, pp. 1-6, 2005.
- [22] J. Schlaich, R. Bergermann, W. Schiel, G. Weinrebe, "Design of commercial solar updraft tower systems-utilization of solar induced convective flows for power generation", Journal of Solar Energy Engineering, vol. 127 (1), pp. 117-124, 2005.
- [23] P. Rodrigo, R. Velazquez, E. Fernandez, F. Almonacid, and A. Lay-Ekuakille, "A method for the outdoor thermal characterisation of high-concentrator photovoltaic modules alternative to the IEC 62670-3 standard", Energy, vol. 148, pp. 159-168, 2018.
- [24] W. Haaf, K. Friedrich, G. Mary, J. Schlaich, "Solar chimney – Part I: Principle and construction of the pilot plant in Manzanares", Int. Journal of Solar Energy, vol. 2 (1), pp. 3-20, 1983.
- [25] W. Haaf, "Solar chimney – Part II: Preliminary test results from the Manzanares pilot plant", Int. Journal of Solar Energy, vol. 2 (2), pp. 141-161, 1984.
- [26] M. O. Hamdan, "Analysis of a solar chimney power plant in the Arabian Gulf region", Renewable Energy, vol. 36, pp. 2593-2598, 2011.
- [27] R. Mazen, M. Radwan, M. Abdel-Samiea, "Solar updraft chimney systems in high rise buildings", in Proc. of IEEE International Conference on Clean Electrical Power, Alghero, pp. 724-727, 2013.
- [28] Devashish, A. Thakur, "A Comprehensive Review on Wind Energy System for Electric Power Generation: Current Situation and Improved Technologies to Realize Future Development", Int. Journal of Renewable Energy Research, vol. 7 (4), 2017.
- [29] M. S. Aziz, S. Ahmed, U. Saleem, G. M. Mufti, "Wind-hybrid Power Generation Systems Using Renewable Energy Sources-A Review", Int. Journal of Renewable Energy Research, vol. 7 (1), 2017.
- [30] B. Shalavadi, V. Ravindranadh, R. Y. Udaykumar, "Modelling and Analysis of a Standalone PV/Micro Turbine/ Ultra Capacitor Hybrid System", Int. Journal of Renewable Energy Research, vol. 6 (3), 2016.
- [31] H. Parsa, N. Maftouni, "Optimization of a Real Scale Shrouded Wind Turbine Using 3D CFD Analysis", Int. J. of Renewable Energy Research, vol. 10 (2), 2020.
- [32] Danish Wind Industry Association, Wind Energy Reference Manual, May 2003. Available Online: <http://xn--drmstrre-64ad.dk/wp-content/wind/miller/windpower%20web/en/stat/units.htm>
- [33] M. N. Eskander and S. I. Amer, "Mitigation of voltage dips and swells in grid-connected wind energy conversion systems", IETE Journal of Research, vol. 57 (6), pp. 515-524, 2014.

- [34] K. S. Dahl and P. Fuglsang, "Design of the wind turbine airfoil family RISØ-A-XX", Risø National Laboratory, ISBN: 87-550-2356-8, Denmark, 1998.
- [35] D. M. Eggleston, F. Stoddard, "Wind Turbine Engineering Design", Van Nostrand Reinhold Co. Inc., New York, USA, 1987.
- [36] E. Assareh, M. Biglari, "A novel approach to capture the maximum power generation from wind turbines using hybrid MLP neural network and bees algorithm (HNNBA)", IETE Journal of Research, vol. 62 (3), pp. 368-378, 2016.
- [37] C. Sanchez, J.E. Zarate, R. Velazquez, S. Sassi, "Analysis of wind missing data for wind farms in Isthmus of Tehuantepec", Proc. of IEEE Int. Autumn Meeting on Power, Electronics Computing, Ixtapa, 2018, pp. 1-6.
- [38] A. Cowen, B. Hardy, R. Mahadevan, S. Wilcenski, "Poly MUMPS Design Handbook: a MUMPs process", Memscap Inc., Revision 13.0, 2011. Available Online: [http://www.memscapinc.com/\\_data/assets/pdf\\_file/001\\_9/1729/PolyMUMPs-DR-13-0.pdf](http://www.memscapinc.com/_data/assets/pdf_file/001_9/1729/PolyMUMPs-DR-13-0.pdf)
- [39] D. Huang, M.A. Reschchikov, P. Visconti, F. Yun, A. Baski, H. Morkoc, C. W. Litton, "Comparative study of Ga and N-polar GaN films grown on sapphire substrates by molecular beam epitaxy" Journal of Vacuum Science and Technology B, vol. 20 (6), pp. 2256 – 2264, 2002.
- [40] J. Varona, M. Tecpoyotl-Torres, and A.A. Hamoui, "Design of MEMS vertical-horizontal chevron thermal actuators", Journal of Sensors & Actuators: A. Physical, vol. 153 (1), pp. 127-130, 2009.
- [41] P. Visconti, D. Huang, M. A. Reschchikov, F. Yun, A. Baski, R. Cingolani, C. Litton, J. Jasinski, Z. L. Weber, H. Morkoc, "Investigation of Defects and Polarity in GaN using hot wet Etching, Atomic Force and Transmission Electron Microscopy and Convergent Beam Electron Diffraction" Physica Status Solidi (b), vol. 228 (2), pp. 513-517, 2001.
- [42] D. Pisignano, L. Persano, E. Mele, P. Visconti, M. Anni, G. Gigli, R. Cingolani, G. Barbarella, "First-order imprinted organic distributed feedback lasers"; Synthetic Metals, vol. 153 (1-3), pp. 237 - 240, 2005.
- [43] D. Pisignano, L. Persano, G. Gigli, P. Visconti, Stomeo, M. De Vittorio, G. Barbarella, R. Cingolani; "Planar organic photonic crystals fabricated by soft lithography". Nanotechnology, vol. 15, pp. 766-770, 2004.
- [44] S. D'Amico, G. Maruccio, P. Visconti, E. D'Amone, A. Bramanti, R. Cingolani, R. Rinaldi; "Ambipolar Transistors based on Azurine Proteins". IEE Proceedings Nanobiotechnology, vol. 151 (5), pp. 173 - 175, 2004.
- [45] H. Fu, X. Chen, I. Shilling, and S. Richardson, "A one-dimensional model for heat transfer in engine exhaust systems" SAE Technical Paper, Number 2005-01-0696, DOI: 10.4271/2005-01-0696, 2005.
- [46] M.J. Sinclair, "A High Force Low Area MEMS Thermal Actuator", IEEE Proc. of 7th Conf. on Thermal & thermo mechanical Phenomena in Electronic Systems, pp. 127-132, DOI: 10.1109/ITHERM.2000.866818, 2000.
- [47] D. Yan, A. Khajepour, R. Mansour, "Modeling of two-hot-arm horizontal thermal actuator", J. of Micromech. and Microengineering, vol. 13 (2), pp. 312-322, 2003.
- [48] P. E. Clark, S. R. Floyd, C. D. Butler, Y. Flom, "Small power technology systems for tetrahedral rovers", A. Inst. of Physics Conf. Proc. vol. 813, pp. 889-897, 2006.
- [49] J. Lueke, W.A. Moussa "MEMS-based power generation techniques for implantable biosensing applications", Sensors, vol. 11 (2), pp. 1433 - 1460, 2011.
- [50] B. Y. Jing, K. S. Leong, "Demonstration of self-powered accelerometer using piezoelectric micro-power generator", In IEEE Proceeding of 2013 Student Conf. on Research and Development (SCOReD), pp. 560 - 563, DOI: 10.1109/SCOReD.2013.7002654, 2015.
- [51] S. Saadon, Y. Wahab, "From ambient vibrations to green energy source: MEMS piezoelectric energy harvester for low frequency application", Proceeding of IEEE Student Symp. in Biomedical Engineering & Sciences (ISSBES), pp. 59 - 63, DOI: 10.1109/ISSBES.2015.7435914, 2015.
- [52] O. Sidek, S. Saadon, "Vibration-based MEMS Piezo electric Energy Harvester for Power Optimization", Proceeding of 15th Int. Conf. on Computer Modelling and Simulation, pp. 241-246, DOI: 10.1109/UKSim.2013.153, 2013.
- [53] F. Herrault, C.H. Ji, M. Allen, "Ultraminiaturized High Speed Permanent-Magnet Generators for Milliwatt-Level Power Generation", J. of Microelectromechanical Systems, vol. 17 (6), pp. 1376 - 1387. 2008.
- [54] M. Kaneko, K. Saito, and F. Uchikoba, "Milliwatt-level electromagnetic induction-type MEMS air turbine generator", Book: MEMS Sensors - Design and Application, Chapter 8, IntechOpen, DOI: 10.5772/intechopen.74830, pp. 171-188, 2018.
- [55] M. Kaneko, K. Mishima, K. Kudo, K. Ebisawa, K. Saito, F. Uchikoba, "Development of mountable electromagnetic induction type MEMS generator", In Proc.of Int. Conf. on Electronics Packaging and iMAPS Asia Conf. ICEP-IAAC, pp. 293-298, DOI: 10.23919/ICEP.2018.8374307, 2018.
- [56] S. K. Nayak and D. N. Gaonkar, "Power management of hybrid fuel cell and microturbine based DG system in utility connected mode," in IEEE Proceeding of 2014 Int. Conference on Renewable Energy Research and Application (ICRERA), Milwaukee, WI, 2014, pp. 342-347, DOI: 10.1109/ICRERA.2014.7016407.
- [57] Y. Yokozeki ; M. Kaneko ; T. Nishi ; H. Endo ; K. Hoshi ; N. Yoshida ; K. Hosoya ; R. Saito ; M. Takato ; K. Saito ; F. Uchikoba, "Electromagnetic induction type micro generator combined with MEMS air turbine and multilayer ceramic magnetic circuit", In Proceeding of Int. Conference on Electronics Packaging (ICEP), pp. 384-387, DOI: 10.1109/ICEP.2014.6826714, 2014.

- [58] V. Rajini, W. M. Amutha, "Real time implementation of a single stage converter based solar-wind hybrid system", in IEEE Proceeding of 2017 6th Int. Conference on Renewable Energy Research and Applications (ICRERA), San Diego, CA, 2017, pp. 1051-1057, DOI: 10.1109/ICRERA.2017.8191218.
- [59] T. S. El-Hasan, "Development of axial flux permanent magnet generator for direct driven micro wind turbine," in IEEE Proceeding of 2016 IEEE Int. Conference on Renewable Energy Research and Applications (ICRERA), Birmingham, 2016, pp. 169-172, DOI: 10.1109/ICRERA.2016.7884531.
- [60] B. S. Jeon, K. J. Park, S.J. Song, Y. C. Joo, K. D. Min, "Design, fabrication, and testing of a MEMS microturbine", Journal of Mechanical Science and Technology, vol. 19, pp. 682 – 691, 2005.
- [61] S. Nagai, K. Tokui, H. Watanabe, J.-I. Itoh, "Wind Turbine Generator Emulator with Current Control mode", in IEEE Proceeding of 2019 8th Int. Conference on Renewable Energy Research and Applications (ICRERA), 3-6 Nov. 2019, Brasov – Romania, pp. 733-738, 2019, DOI: 10.1109/ICRERA47325.2019.8997022.
- [62] A. Iizuka, M. Takato, T. Nishi, K. Saito, F. Uchikoba, "Millimeter Scale MEMS Air Turbine Generator by Winding Wire and Multilayer Magnetic Ceramic Circuit", Modern Mechanical Engineering, vol. 2012 (2), pp. 41 - 46, DOI:10.4236/mme.2012.22006, 2012.
- [63] M. Liamini, H. Shahriar, S. Vengallatore, L. G. Fréchette, "Design Methodology for a Rankine Microturbine: Thermomechanical Analysis and Material Selection", Journal of Microelectromechanical Systems, vol. 20 (1), DOI: 10.1109/JMEMS.2010.2093565, 2011.
- [64] P. Visconti, C. Turco, R. Rinaldi, R. Cingolani, "Nanopatterning of organic and inorganic materials by holographic lithography and plasma etching", Micro electronic Engineering, vol. 53 (1), pp. 391 - 394, 2000.
- [65] H. Raisigel, O. Cugat, M. Delamare, O. Wiss, H. Rostaing, "Magnetic planar micro generator", In Proceedings of 13th Int. Conf. on Solid-State Sensors, Actuators and Microsystems, pp. 757-761, DOI: 10.1109/SENSOR.2005.1496527.
- [66] R. de Fazio, D. Cafagna, G. Marcuccio, A. Minerba, P. Visconti "A Multi-Source Harvesting System Applied to Sensor-Based Smart Garments for Monitoring Workers' Bio-Physical Parameters in Harsh Environments", Energies, vol. 13 (9), pp. 1-33, Article n. 2161, 2020.
- [67] P. Visconti, R. de Fazio, R. Velázquez, C. Del-Valle-Soto, N. I. Giannoccaro; "Development of sensors-based agri-food traceability system remotely managed by a software platform for optimized farm management", Sensors, vol. 20 (13), pp. 1 - 43, Article n. 3632, 2020.